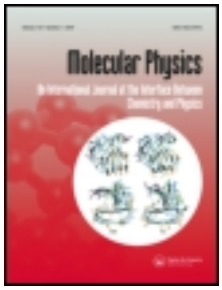

Molecular Physics: An International Journal at the Interface Between Chemistry and Physics
Publication details, including instructions for authors and subscription information:
http://www.tandfonline.com/loi/tmph20

From collisions to clusters: first steps of sulphuric acid nanocluster formation dynamics

Ville Loukonen[a], Nicolai Bork[ab] & Hanna Vehkamäki[a]
[a] Department of Physics, University of Helsinki, Helsinki, Finland
[b] Department of Chemistry, H. C. Ørsted Institute, University of Copenhagen, Copenhagen, Denmark
Published online: 20 Jan 2014.

To cite this article: Ville Loukonen, Nicolai Bork & Hanna Vehkamäki (2014): From collisions to clusters: first steps of sulphuric acid nanocluster formation dynamics, Molecular Physics: An International Journal at the Interface Between Chemistry and Physics, DOI: 10.1080/00268976.2013.877167

To link to this article: http://dx.doi.org/10.1080/00268976.2013.877167

Molecular Physics, 2014
http://dx.doi.org/10.1080/00268976.2013.877167

RESEARCH ARTICLE

From collisions to clusters: first steps of sulphuric acid nanocluster formation dynamics

Ville Loukonen[a,*], Nicolai Bork[a,b] and Hanna Vehkamäki[a]

[a]*Department of Physics, University of Helsinki, Helsinki, Finland;* [b]*Department of Chemistry, H. C. Ørsted Institute, University of Copenhagen, Copenhagen, Denmark*

(*Received 9 September 2013; accepted 12 December 2013*)

The clustering of sulphuric acid with base molecules is one of the main pathways of new-particle formation in the Earth's atmosphere. First step in the clustering process is likely the formation of a (sulphuric acid)$_1$(base)$_1$(water)$_n$ cluster. Here, we present results from direct first-principles molecular dynamics collision simulations of (sulphuric acid)$_1$(water)$_{0,1}$ + (dimethylamine) → (sulphuric acid)$_1$(dimethylamine)$_1$(water)$_{0,1}$ cluster formation processes. The simulations indicate that the sticking factor in the collisions is unity: the interaction between the molecules is strong enough to overcome the possible initial non-optimal collision orientations. No post-collisional cluster break up is observed. The reasons for the efficient clustering are (i) the proton transfer reaction which takes place in each of the collision simulations and (ii) the subsequent competition over the proton control. As a consequence, the clusters show very dynamic ion pair structure, which differs from both the static structure optimisation calculations and the equilibrium first-principles molecular dynamics simulations. In some of the simulation runs, water mediates the proton transfer by acting as a proton bridge. In general, water is able to notably stabilise the formed clusters by allocating a fraction of the released clustering energy.

Keywords: molecular collisions; first-principles molecular dynamics; atmospheric new-particle formation

1. Background

The significance of sulphuric acid (H_2SO_4, henceforth SA) in atmospheric new-particle formation has been well established [1,2]. Similarly, the need for other participating species in the initial clustering and during the subsequent growth processes is well documented in the literature [3]. However, the exact details of the new-particle formation process are still to be revealed. Recently, an acid–base stabilisation mechanism involving dimethylamine ($(CH_3)_2NH$, henceforth DMA) as the base molecule has been discussed in some detail [4–8]. In essence, the crux of the argument is that SA and DMA form very stable clusters due to proton transfer reactions which are assumed to take place in the process. In addition to calculations performed on various levels of computational sophistication, the argument is strengthened by experimental studies on the enhancing effect of the amines on the new-particle formation [9–12].

A vast majority of the recent theoretical investigations on atmospheric new-particle formation are based on the standard electronic structure calculations procedure (for details, see [13]). In this scheme, one typically seeks the most stable molecular cluster at the temperature $T = 0$ K and then extrapolates to ambient temperatures using the harmonic oscillator–rigid rotor approximation (HORRA). This also entails the assumption of the thermodynamical equilibrium. However, molecular clustering is a very dynamic non-equilibrium phenomenon, and it is debatable to what extent it can be approximated relying on equilibrium concepts. For example, the described standard procedure simplifies the entire statistical mechanical phase space into one or few energetically favourable cluster configurations. This is a drastic approximation and it is known to worsen with increasing temperature and complexity of the system [14,15]. Typically, the approximation is applied only out of computational necessity – sophisticated phase-space sampling methods [16–18] often require at least $\mathcal{O}(10^6)$ energy evaluations per cluster, which is a very significant computational burden, especially at an *ab initio* level. Free energy calculations based on the standard electronic structure procedure are further challenged by the HORRA. Similarly with the previous approximation, the HORRA also worsens as the complexity and temperature of the system grow [14,15,19]. Ideally, theoretical investigations of molecular clustering would take into account both of the described non-ideal contributions. Essentially, this means solving the quantum many-body dynamics for both the electrons and atomic nuclei present in the system. Even with the full power of the current high-performance supercomputers, this goal is still far unattainable. Thus, a practical scientist must seek for a more affordable method to study the phenomenon – a method that is hopefully

* Corresponding author. Email: ville.loukonen@helsinki.fi

not ridden with the discussed approximations. Besides Monte Carlo approaches, one such method is the molecular dynamics simulation.

On a larger scale force-field molecular dynamics simulations have been successfully used to obtain insight into various dynamic physical quantities and features such as the mass accommodation factor [20,21], collision cross-sections [22,23] and post-collisional relaxation of small clusters [24,25]. Unfortunately, the force-field molecular dynamics simulations provide only crude approximations if used to study the first steps of SA-driven new-particle formation due to the very high reactivity of the acid. Thus, one is forced to use a method which is able to account for the changes in the electronic structure of the system on the fly. One method meeting the discussed criteria is the first-principles molecular dynamics (FPMD) simulation. Recently, the applicability of the FPMD simulation to study atmospherically relevant collision processes was demonstrated [26], and here we take the first steps towards investigating the molecular-level dynamics behind the SA clustering process.

We present results from direct FPMD collision simulations for the clustering of (SA) + (DMA) → (SA)(DMA) and (SA)(water) + (DMA) → (SA)(DMA)(water). In atmospheric conditions, most of the SA is most likely hydrated by at least one water molecule [27,28]. This follows from the fact that there are typically 10^{10} times more water than sulphuric acid molecules in the atmosphere. Although the bonding of water with SA is considerably weaker than that with DMA, it is thus essential to study the role of water during the initial clustering.

Above all, this straightforward approach allows the investigation of the sticking factor: can non-optimal collision geometry hinder or prevent the clustering – or can water block the reaction? Furthermore, FPMD simulations reveal the dynamics of the collision: does the proton transfer always happen – or can the transferred proton transfer back to the acid?

These questions are answered in detail in Section 3. First, the technical simulation details are given in Section 2. Discussion concerning the consequences of the results then closes the paper in Section 4.

2. Collision simulations

To probe the dynamics of the (SA)(DMA) and the (SA)(DMA)(water) cluster formation, we performed 12 direct head-on collisions for both the clusters. By varying the starting geometries, we tried to accommodate all the relevant head-on collision possibilities (see Supplemental data Figure S2 and Figure S3 for all the initial collision geometries). Due to the high computational cost (see below), we were only able to study head-on collisions.

The collisions were performed using the Born–Oppenheimer FPMD simulation method with the CP2K program package [29]. We applied the Perdew–Burke–Ernzerhof (PBE) density functional [30] with the dispersion correction D3 devised by Grimme [31]. Recent benchmarking studies [32,33] found the PBE functional to perform quite well for various sulphuric acid containing clusters, especially when used with the dispersion correction. We used an augmented doubly polarised triple-ζ Gaussian-type basis set in the real space together with a plane-wave basis set of cut-off 400 Ry in the momentum space [34]. Norm-conserving Goedecker–Teter–Hutter (GTH) pseudo-potentials were used for the core electronic states [35], and the convergence criterion for the wave-function was 10^{-7} Hartrees. The collisions were performed in a simulation box of $20 \times 20 \times 20$ Å^3, where periodic boundary conditions were not applied in any direction. The Poisson equation was solved according to the scheme by Martyna and Tuckerman [36]. The collisions were run in the *NVE* ensemble.

In all the simulations, a time step of 0.5 fs was used. On the average, we were able to perform one simulation time step in about 0.4 CPU-hours. Given this high computational burden, we chose the initial collision velocities to be roughly twice the relative velocity between the species according to the Maxwell–Boltzmann distribution at a temperature of $T = 300$ K to be able to perform as many collisions as possible and to run the simulations sufficiently long after the collisions. Sensitivity testing revealed that the elevated collision velocities did not change the collision dynamics, but made the molecules collide faster, as desired. The (SA)+(DMA) collisions were let to run for 5 picoseconds (ps) and the (SA)(water)+(DMA) collision for 7 ps.

In addition to the collisions, we also performed equilibrium FPMD simulations for the two clusters, (SA)(DMA) and (SA)(DMA)(water) (cf. Section 3.4). These simulations were performed with the same technical details and at the same level of theory as the collisions, except now in the *NVT* ensemble at a temperature of $T = 300$ K. Each degree of freedom was controlled by a Nosé–Hoover chain thermostat with a coupling constant of 2000 cm^{-1} [37]. The initial cluster configurations were taken from the literature [5] and first optimised with the level of theory used here. Then, the clusters were equilibrated for 3 ps and the data were collected during production runs of 8 ps.

3. Results of the collision simulations

3.1. *Sticking factor = 1*

Perhaps the first thing to observe in the collisions of molecules is whether or not the species stick together – do the molecules bond in such a way they can be said to form a small cluster? If the sticking factor for the (SA) + (DMA) collision significantly differs from unity, it is likely to alter the clustering efficiency, as the formation of the (SA)(DMA) cluster seems to be the very first step in the

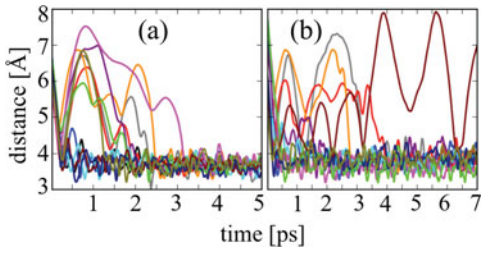

Figure 1. The distance between the centre-of-mass (SA) and centre-of-mass (DMA) in the simulation runs. (a) (SA) + (DMA) → (SA)(DMA) collisions; (b) (SA)(water) + (DMA) → (SA)(DMA)(water) collisions. The distances are given in Å and the time in ps. One (SA)(water)+(DMA) collision took longer (∼9 ps) to find a sticking configuration (see text). Here the centres-of-mass exclude the hydrogens. For more quantitative inspection, a larger figure with a legend is provided in Supplemental data Figure S1.

DMA-enhanced SA clustering process [7]. A suitable metric for the sticking can be obtained from the simulations by monitoring the positions of the centres-of-mass of the molecules. In Figure 1, the distance between the centre-of-mass of the SA and the centre-of-mass of the DMA is shown for each simulation run: in the graph (a) for the (SA) + (DMA) → (SA)(DMA) collisions and in the graph (b) for the (SA)(water) + (DMA) → (SA)(DMA)(water) collisions. Figure 1(a) reveals immediately that there is no significant steric hindrance in the (SA) + (DMA) collisions: non-optimal collision geometry is always overcome within roughly 3 ps. Six of the total 12 collisions lead directly to a cluster within 1 ps. In the other half of the collisions, structural rearrangement is needed before the cluster formation. See Supplemental data Figure S2 for the initial collision geometries.

Very similar conclusions can be drawn from the (SA)(water) + (DMA) collisions. Eleven of the total 12 collisions result in sticking within 4 ps, nine of these already within 2 ps. However, one collision simulation did not stick during the 7 ps of simulation. As the initial structure of the collision in question intuitively looks particularly susceptible for proton transfer, the simulation was continued. After 9 ps, also this simulation led to a bound cluster (see Supplemental data Figure S1 for the sticking and Figure S3 for the initial collision geometries).

Although an FPMD simulation is a very powerful method, care must be taken in the physical interpretation of the results. Inadequate phase-space sampling may lead to an unsatisfactory description of the underlying dynamics. Fortunately, the head-on collisions under investigation here appear to be an on/off system. Besides showing that there is no steric hindrance in the cluster formation, this is demonstrated in Figure 1: after the collisions the molecules stay bound together as a cluster. In neither set of the simulations do the molecules break back to separated monomers (or into a monomer and a dimer). This is due both to the strong ion-enhanced hydrogen bonding, which results from the proton transfer, and to the large enough number of accessible degrees of freedom, which are able to accommodate the energy released in the clustering process.

3.2. *Proton transfer happens always*

In all of the collision simulations, a proton transfer takes place, both in the runs with and without water. The instant in time the proton transfer takes place is highlighted by the maroon vertical lines running through all the subplots in Figures 2 and 3. The dynamics of the transfer are shown by the red curves in the uppermost graphs of each subplot in Figures 2 and 3. These curves show the difference between the distance from the transferred proton to the oxygen it is initially bound (R_{OH}) and to the nitrogen (R_{NH}) which captures it,

$$R_{trans} = R_{OH} - R_{NH}. \quad (1)$$

Thus, the proton transfer is defined to happen when the R_{trans} becomes positive. After the proton transfer, the R_{OH} tracks the distance from the transferred proton to the closest of the SA's oxygens, which is not necessarily the same oxygen it was initially bound to. All the proton transfers in the (SA)+(DMA) collisions and most of the transfers in the (SA)(water) + (DMA) collisions are direct: the proton transfers directly from the SA's oxygen to the DMA's nitrogen atom. However, in five of the collisions including water, the molecular arrangement was such that the direct transfer was not favourable. Basically, the nitrogen's lone pair electrons were too far from both of the SA's hydrogens to induce the reaction. In these cases, the water molecule acts as a proton bridge and the reaction proceeds via Grotthuss-type mechanism. The water transfers a proton to the DMA at the same time as it receives another proton from the SA (cf. Figure 4). The reaction proceeds very rapidly, within 100 fs. Effectively, the water stays as a neutral molecule, just mediating the ion pair formation. After the proton transfer, the electrostatic attraction between HSO_4^- and $(CH_3)_2NH_2^+$ pulls the ions in contact, pushing the water farther away. In Figure 3(b), the evolution of the proton bridge process is shown by the orange curve in the uppermost subplots: the curve shows the differences in the distances measured from the transferred proton similarly to the R_{trans}, but here between the water and the DMA (all the proton bridge processes are shown similarly in Supplemental data Figure S3).

3.3. *The release of energy in the proton transfer is significant*

The potential and the kinetic energies of the (SA) + (DMA) simulations are shown in Figure 2 and for the (SA)(water) + (DMA) collisions in Figure 3: in each subplot the black curve in the middle panel shows the potential energy of the

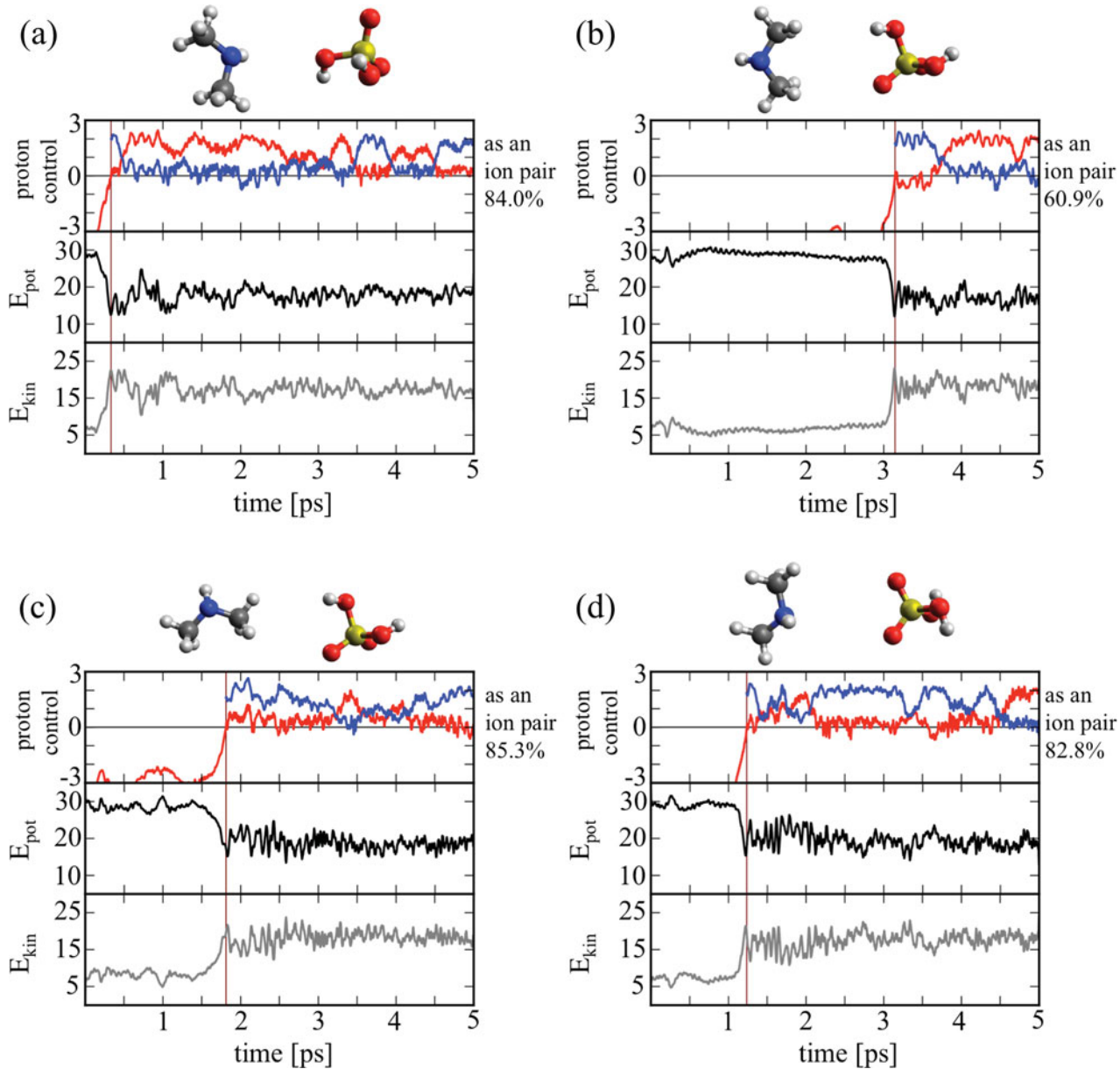

Figure 2. Proton control and the energetics for representative (SA) + (DMA) → (SA)(DMA) collisions. In each graph, the uppermost panel shows the proton control. The red curve (initially negative) shows the proton transfer distance R_{trans} and the blue curve (beginning at the proton transfer; denoted by the vertical lines) corresponds to hydrogen bonding competition R_{comp} in Å (see Equations (1) and (2)). When both the red and blue curves are positive, the system is an ion pair; the percentages of the simulation time the cluster spends as an ion pair after the initial proton transfer are given next to the proton control graphs. The middle panel shows the evolution of the potential energy E_{pot} and the bottommost panel the evolution of the kinetic energy E_{kin} of the whole system. The energies are given in units of kcal/mol. The E_{pot} is measured with respect to the optimised cluster at $T = 0$ K, and the E_{kin} is the total kinetic energy of the system in the centre-of-mass frame. For each run, the initial molecular collision geometry is shown; sulphur atoms are depicted in yellow, oxygens in red, nitrogens in blue, carbons in grey and hydrogens in white.

whole system; the corresponding kinetic energy is shown in the bottommost panel by the grey curve. The potential energy consists of both the intra- and inter-molecular contributions, and is given with reference to the optimised ground-state energies of the clusters at $T = 0$ K. The kinetic energy is given with respect to the centre-of-mass of the cluster. There is a distinctive drop in the potential energy when the proton transfer happens. Coinciding with this, the kinetic energy of the system naturally increases. The average change in the energy caused by the proton transfer in the (SA) + (DMA) collisions is 8.6 ± 1.8 kcal/mol and in the (SA)(water) + (DMA) collisions, 8.0 ± 2.3 kcal/mol

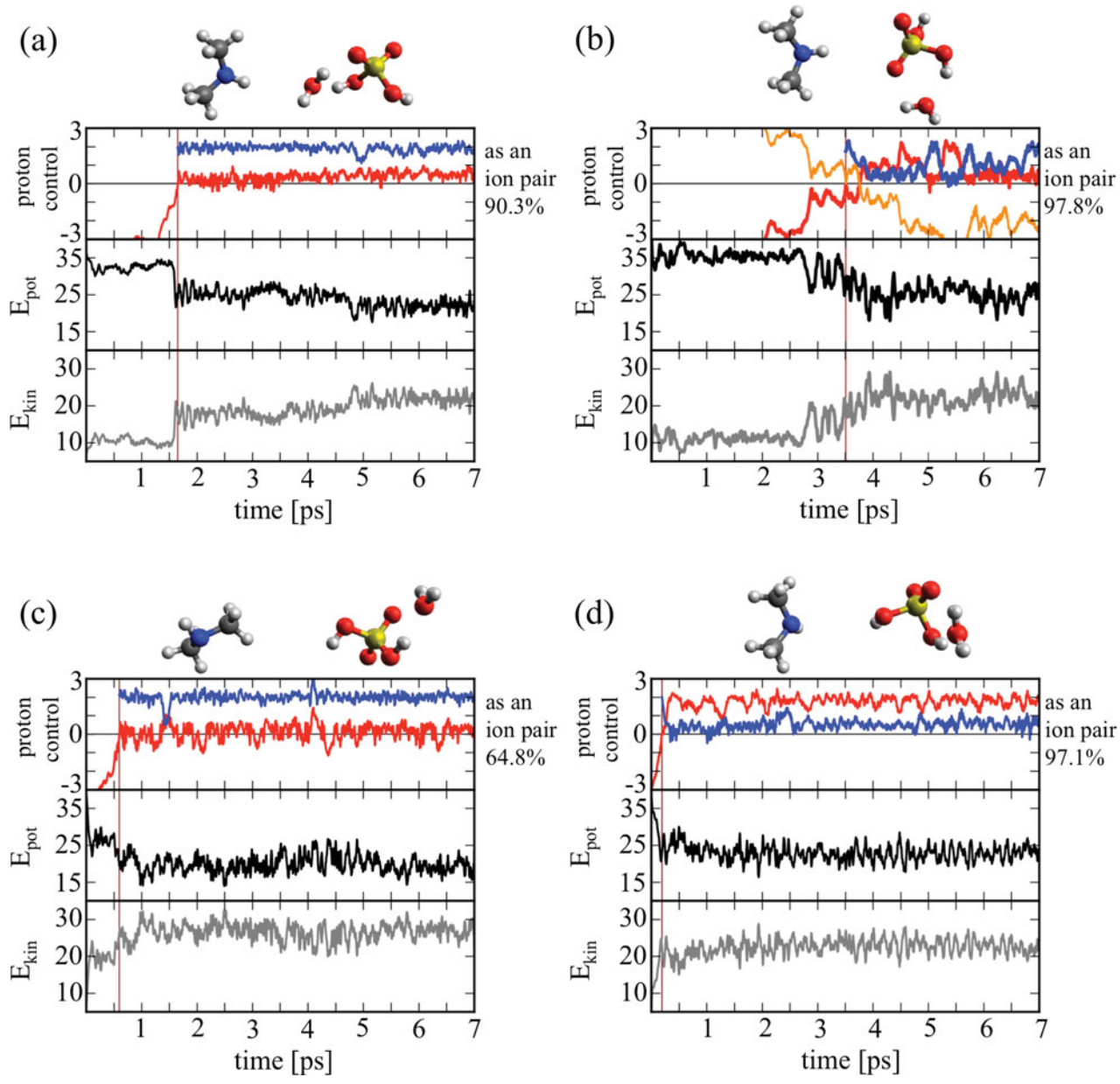

Figure 3. Proton control and the energetics for representative (SA)(water) + (DMA) → (SA)(DMA)(water) collisions. In each graph, the uppermost panel shows the proton control. The red curve (initially negative) shows the proton transfer distance R_{trans} and the blue curve (beginning at the proton transfer; denoted by the vertical lines) corresponds to hydrogen bonding competition R_{comp} in Å (see Equations (1) and (2)). When both the red and blue curves are positive, the system is an ion pair; the percentages of the simulation time the cluster spends as an ion pair after the initial proton transfer are given next to the proton control graphs. In graph (b), the orange curve (initially positive) shows the proton bridge mechanism. The middle panel shows the evolution of the potential energy E_{pot} and the bottommost panel the evolution of the kinetic energy E_{kin} of the whole system. The energies are given in units of kcal/mol. The E_{pot} is measured with respect to the optimised cluster at $T = 0$ K, and the E_{kin} is the total kinetic energy of the system in the centre-of-mass frame. For each run, the initial molecular collision geometry is shown; sulphur atoms are depicted in yellow, oxygens in red, nitrogens in blue, carbons in grey and hydrogens in white.

(averaged over all the runs). This is a considerable amount of energy in the context of small hydrogen-bonded clusters. The released energy keeps the clusters kinetically exited, but importantly is not enough to break the clusters back into monomers (or into a monomer and a dimer), as can be seen in Figures 1, 2 and 3. Also, from the potential and kinetic energy curves in Figures 2 and 3, one can see that in most of the simulation runs the oscillation in the energy relaxes in roughly 1 ps after the proton transfer as more of the accessible degrees of freedom become exited.

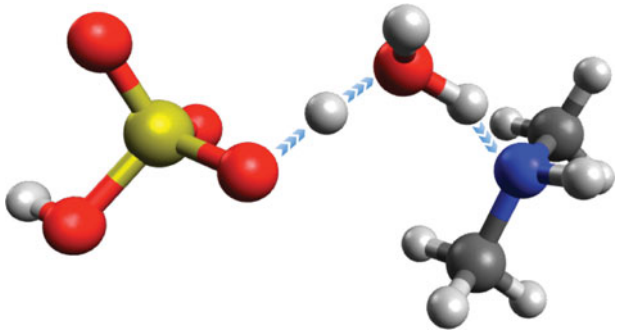

Figure 4. One example of water acting as a proton bridge and mediating the ion pair formation. The proton initially held by the SA is transferring to the water molecule, and one of the water's protons is starting to transfer to the DMA. Colours are as in Figures 2 and 3. The depicted frame corresponds to the simulation run shown in Supplemental data Figure S3(e) at the time 3.058 ps.

On a microscopic scale, the kinetic energy translates into molecular movement. Here, the kinetic energy in the newly formed clusters is bound to have an effect on the bonding. However, the further fate of the clusters is difficult to predict based solely on the presented simulations. After the formation of the studied clusters in the atmosphere, the vast overwhelming majority of the subsequent collisions the clusters undergo will be with inert carrier gas molecules. Assuming a sulphuric acid concentration of 10^6 per cm^3, the clusters collide with the acid monomer roughly once in 4 minutes, whereas they will encounter a carrier gas molecule once in 80 ps under 1 atm pressure and a temperature of 300 K. Dedicated collision simulations investigating the energy transfer between the newly formed clusters and the carrier gas would give valuable insight into the relaxation timescale – however, such simulations are beyond the scope of the current paper.

3.4. *Proton control differs from the equilibrium*

The efficient clustering between DMA and SA (and water) results from the initial proton transfer from SA to DMA and from the subsequent competition over the control of the two protons involved in the bonding. In addition to showing the proton transfer distances R_{trans}, the uppermost graphs in Figures 2 and 3 also show the proton control competition between the SA and DMA. The blue curves in the subplots show the difference in distances from the proton initially bound to DMA to DMA's nitrogen (R'_{NH}) and to SA's closest oxygen atom (R'_{OH}):

$$R_{\text{comp}} = R'_{\text{OH}} - R'_{\text{NH}}. \quad (2)$$

Defined in this way, the positive values correspond to DMA controlling the proton, similarly to the proton transfer distances R_{trans}, shown in red in the same graphs. A combination of these curves thus gives the total picture of the proton control: when both the curves are positive at the same time, DMA controls both protons and consequently, the cluster is an ion pair. Instances where either R_{trans} or R_{comp} is negative correspond to nominally neutral molecules bound by one or more hydrogen bonds. In Figures 2 and 3, the percentage of the time the clusters spend as ion pairs after the initial transfer is given next to the proton control graphs for each collision simulation.

The first aspect to notice is the very dynamic nature of the bonding between the molecules. The proton transfer and the following bonding is far from static. On the average, the (SA)(DMA) cluster is an ion pair 76% ± 8% of the time after the initial proton transfer. The static structure optimisation calculations also predict proton transfer in the (SA)(DMA) clusters [4,5] as reported in the current paper. However, by the nature of these static calculations, no dynamical effects are taken into account. Consequently, all further analysis based on the static calculations implicitly assumes that the cluster of (SA)(DMA) spends 100% of the time as an ion pair. In light of the results presented here, this assumption might be a significant source of error, for example, in the free energy calculations. On the other hand, the cluster analysis based on the structure optimisation calculations typically assumes also that the thermodynamic equilibrium prevails. To obtain insight into the behaviour of the clusters in equilibrium, we simulated the clusters in the *NVT* ensemble at $T = 300$ K, starting directly from the minimum energy structures (cf. simulation details in Section 2). The energetics and proton control of these simulations are shown in Figure 5. In the case of the (SA)(DMA) cluster, the 8 ps equilibrium simulations reveal that the cluster spends 93% of the time as an ion pair (cf. Figure 5(a)). Two interesting conclusions can be drawn. First, the assumption that the cluster of (SA)(DMA) is always an ion pair is not valid and is likely to induce errors in the energetics based on the static calculations, especially if only the most stable configuration is taken into account. Second, the proton control dynamics of the (SA)(DMA) cluster differ significantly between the collision and equilibrium simulations. The reason for this is the released energy in the proton transfer which turns into kinetic energy. To reach equilibrium, the cluster needs to dispose the extra energy. Likely, this will happen via collisions with the carrier gas, as discussed in Section 3.3.

The inclusion of one water molecule changes the proton control dynamics. Based on the collision simulations, the (SA)(DMA)(water) cluster is an ion pair 88% ± 12% of the time after the initial proton transfer. Clearly, water is able to stabilise the ion pair dynamics. The water molecule provides additional degrees of freedom which can allocate some of the kinetic energy within the system. The change in the proton control percentage from the (SA)(DMA) case is quite significant. This can be also distinctively seen by comparing the proton control graphs in Figures 2 and 3: the R_{trans} and R_{comp} curves are much smoother and the oscillation is more restrained in the case of (SA)(DMA)(water) clusters.

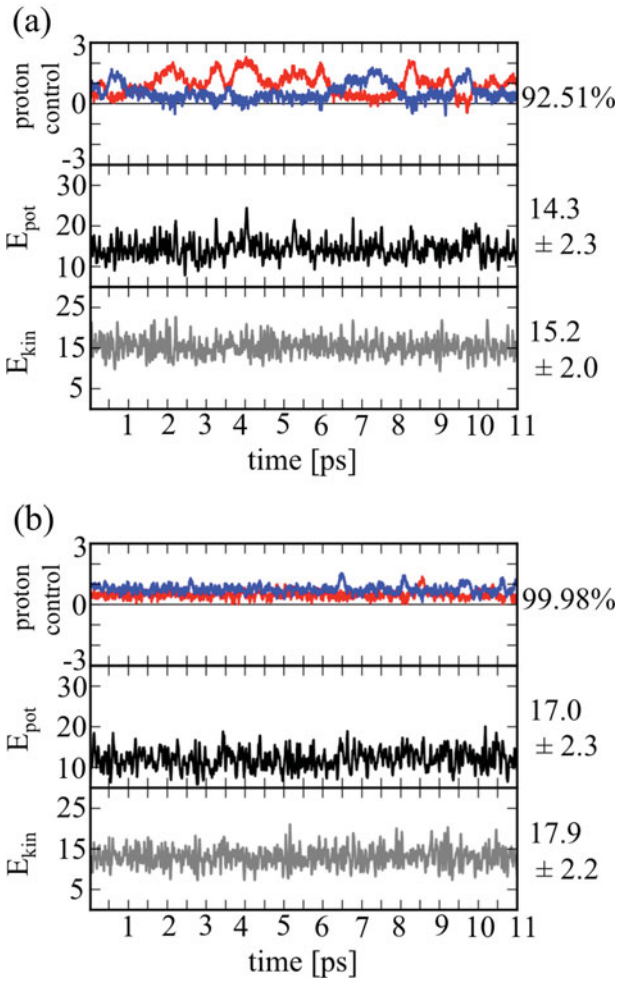

Figure 5. Proton control (in Å) and the energetics (in kcal/mol) of the equilibrium simulations at the temperature of $T = 300$ K; (a) (SA)(DMA), (b) (SA)(DMA)(water). The potential energies E_{pot} are given with respect to the optimised structures. The first 3 ps of the simulations were used to equilibrate the clusters and data was collected during the last 8 ps. The mean values (with standard deviations) are given next to the energies from the last 8 ps together with the proton control percentages. Here the proton control curves (blue and red) show the differences in the distances from the two protons to the DMA's nitrogen and to the closest oxygen atom of the SA or water. As in Figures 2 and 3, positive values correspond to the DMA controlling the protons.

The stabilising effect of water is even more pronounced in the equilibrium simulation at $NVT(T = 300$ K) (cf. Figure 5(b)). The equilibrium simulation agrees well with the static calculations with regard to the proton control, giving 99.98% ion pair percentage for the cluster, as also the static structure optimisation calculations predict the proton transfer [5]. According to the results presented here, we can conclude that the (SA)(DMA)(water) cluster has an ion pair structure under thermodynamical equilibrium at $T =$ 300 K. However, to obtain equilibrium after the collisional formation, the cluster still needs to dispose some of the extra energy, similarly to the (SA)(DMA) cluster. It should also be stressed that although the ion pair percentage of the (SA)(DMA)(water) cluster in equilibrium simulations is practically the same as in the static calculations, there are features in the cluster energetics which go beyond the static approach. For example, Figure 5 shows that the average potential and kinetic energies are not equal in the equilibrium simulation, indicating that the vibrational motion of the clusters is not harmonic [15]. The same applies also to the (SA)(DMA) cluster.

4. Conclusions and discussion

The reported direct FPMD collision simulations present the first steps in deeper and more detailed understanding of atmospheric clustering. The simulations indicate that the proton transfer will always take place in the head-on collisions between SA and DMA, resulting in relatively strongly bound clusters. The presence of one water molecule or non-optimal initial collision geometry is not enough to hinder the reaction. The released energy in the proton transfer keeps the clusters kinetically exited, leading to ion pair cluster structures differing from equilibrium considerations. The existence of water is observed to stabilise the cluster as it can accommodate a portion of the kinetic energy. The stabilising effect of water is in agreement with the previous equilibrium FPMD simulations [15], where already the cluster of $(SA)_2(DMA)_1$ was seen to be an ion pair 100% of the simulation time. Together, these simulation results suggest that the ion pair structure is likely to be conserved when the system possesses an ample amount of degrees of freedom. This in turn implies that the possible cluster reorganisation after collisions happens via ion pairs, and that fragmentation is more likely cluster process than SA monomer evaporation – given that there are enough base molecules to accommodate the proton transfer.

The presented direct collision simulations also indirectly hint at the importance of the entropic contributions to the formation free energies. The observed dynamical nature of the ion pairs is likely to have a contribution to the formation energetics – a contribution which is beyond the reach of the standard electronic structure calculations with the HORRA. Instead, formation free energies based on more complete phase-space sampling with anharmonic motion are called for. For example, thermodynamic integration or metadynamics with FPMD simulations as a physics engine fulfil these requirements; these possibilities will be explored in the future endeavours.

Acknowledgements

We gratefully acknowledge the financial support by the Maj and Tor Nessling Foundation (project #2011200), the Academy of Finland (Center of Excellence program, project #1118615, and LASTU program, project #135054), the European Research Council (project #257360 MOCAPAF) and the Villum Foundation. We also thank the CSC – IT Center for Science Ltd. and the University of Helsinki for providing computational resources.

Supplemental data

Supplemental data for this article can be accessed here.

References

[1] M. Kulmala, H. Vehkamäki, T. Petäjä, M. Dal Maso, A. Lauri, V.-M. Kerminen, W. Birmili, and P.H. McMurry, Aerosol Sci. **35**, 143 (2004).

[2] C. Kuang, P.H. McMurry, A.V. McCormick, and F.L. Eisele, J. Geophys. Res. **113**, D10209 (2008).

[3] R. Zhang, Science **328**, 1366 (2010).

[4] T. Kurtén, V. Loukonen, H. Vehkamäki, and M. Kulmala, Atmos. Chem. Phys. **8**, 4095 (2008).

[5] V. Loukonen, T. Kurtén, I.K. Ortega, H. Vehkamäki, A.A.H. Pádua, K. Sellegri, and M. Kulmala, Atmos. Chem. Phys. **10**, 4961 (2010).

[6] J.W. DePalma, B.R. Bzdek, D.J. Doren, and Murray V. Johnston, J. Phys. Chem. A **116**, 1030 (2012).

[7] M.J. McGrath, T. Olenius, I.K. Ortega, V. Loukonen, P. Paasonen, T. Kurtén, M. Kulmala, and H. Vehkamäki, Atmos. Chem. Phys. **12**, 2345 (2012).

[8] I.K. Ortega, O. Kupiainen, T. Kurtén, T. Olenius, O. Wilkman, M.J. McGrath, V. Loukonen, and H. Vehkamäki, Atmos. Chem. Phys. **12**, 225 (2012).

[9] J.N. Smith, K.C. Barsanti, H.R. Friedli, M. Ehn, M. Kulmala, D.R. Collins, J.H. Scheckman, B.J. Williams, and P.H. McMurry, Proc. Natl. Acad. Sci. **107**, 6634 (2010).

[10] J. Zhao, J.N. Smith, F.L. Eisele, M. Chen, C. Kuang, and P.H. McMurry, Atmos. Chem. Phys. **11**, 10823 (2011).

[11] J.H. Zollner, W.A. Glasoe, B. Panta, K.K. Carlson, P.H. McMurry, and D.R. Hanson, Atmos. Chem. Phys. **12**, 4399 (2012).

[12] J. Almeida, S. Schobesberger, A. Kürten, I.K. Ortega, O. Kupiainen–Määttä, A.P. Praplan, A. Adamov, A. Amorim, F. Bianchi, M. Breitenlechner, A. David, J. Dommen, N.M. Donahue, A. Downard, E. Dunne, J. Duplissy, S. Ehrhart, R.C. Flagan, A. Franchin, R. Guida, J. Hakala, A. Hansel, M. Heinritzi, H. Henschel, T. Jokinen, H. Junninen, M. Kajos, J. Kangasluoma, H. Keskinen, A. Kupc, T. Kurtén, A.N. Kvashin, A. Laaksonen, K. Lehtipalo, M. Leiminger, J. Leppä, V. Loukonen, V. Makhmutov, S. Mathot, M.J. McGrath, T. Nieminen, T. Olenius, A. Onnela, T. Petäjä, F. Riccobono, I. Riipinen, M. Rissanen, L. Rondo, T. Ruuskanen, F.D. Santos, N. Sarnela, S. Schallhart, R. Schnitzhofer, J.H. Seinfeld, M. Simon, M. Sipilä, Y. Stozhkov, F. Stratmann, A. Tomé, J. Tröstl, G. Tsagkogeorgas, P. Vaattovaara, Y. Viisanen, A. Virtanen, A. Vrtala, P.E. Wagner, E. Weingartner, H. Wex, C. Williamson, D. Wimmer, P. Ye, T. Yli-Juuti, K.S. Carslaw, M. Kulmala, J. Curtius, U. Baltensperger, D.R. Worsnop, H. Vehkamäki, and J. Kirkby, Nature **502**, 359 (2013).

[13] T. Kurtén and H. Vehkamäki, Adv. Quant. Chem. **55**, 407 (2008).

[14] S. Kathmann, G. Schenter, and B. Garrett, J. Phys. Chem. C **111**, 4977 (2007).

[15] V. Loukonen, I-F.W. Kuo, M.J. McGrath, and H. Vehkamäki, Chem. Phys. **428**, 164 (2014).

[16] B. Chen and J.I. Siepmann, J. Phys. Chem. B **104**, 8725 (2000).

[17] B. Chen, J.I. Siepmann, and M.L. Klein, J. Phys. Chem. A **109**, 1137 (2005).

[18] S.M. Kathmann, G.K. Schenter, B.C. Garrett, B. Chen, and J.I. Siepmann, J. Phys. Chem. C **113**, 10354 (2009).

[19] S.M. Kathmann, G.K. Schenter, and B.C. Garrett, J. Chem. Phys. **116**, 5046 (2002).

[20] X. Ma, P. Chakraborty, B.J. Henz, and M.R. Zachariah, Phys. Chem. Chem. Phys. **13**, 9374 (2011).

[21] J. Julin, M. Shiraiwa, R.E.H. Miles, J.P. Reid, U. Pöschl, and I. Riipinen, J. Phys. Chem. A **117**, 410 (2013).

[22] J. Lengyel, J. Kočišek, V. Poterya, A. Pysanenko, P. Svrčková, M. Fárník, D.K. Zaouris, and J. Fedor, J. Chem. Phys. **137**, 034304 (2012).

[23] I. Napari and H. Vehkamäki, J. Chem. Phys. **120**, 165 (2004).

[24] I. Napari and H. Vehkamäki, J. Chem. Phys. **124**, 024303 (2006).

[25] I. Napari and H. Vehkamäki, J. Chem. Phys. **125**, 094313 (2006).

[26] N. Bork, V. Loukonen, and H. Vehkamäki, J. Phys. Chem. A **117**, 3143 (2013).

[27] T. Kurtén, M. Noppel, H. Vehkamäki, M. Salonen, and M. Kulmala, Boreal Env. Res. **12**, 431 (2007).

[28] B. Temelso, T.E. Morrell, R.M. Shields, M.A. Allodi, E.K. Wood, K.N. Kirschner, T.C. Castonguay, K.A. Archer, and G.C. Shields, J. Phys. Chem. A **116**, 2209 (2012).

[29] Freely available from www.cp2k.org under the GPL license.

[30] J.P. Perdew, K. Burke, and M. Ernzerhof, Phys. Rev. Lett. **77**, 3865 (1996).

[31] S. Grimme, J. Comput. Chem. **27**, 1787 (2006).

[32] J. Elm, M. Bilde, and K.V. Mikkelsen, J. Chem. Theory Comput. **8**, 2071 (2012).

[33] H.R. Leverentz, J.I. Siepmann, D.G. Truhlar, V. Loukonen, and H. Vehkamäki, J. Phys. Chem. A **117**, 3819 (2013).

[34] G. Lippert, J. Hutter, and M. Parrinello, Mol. Phys. **92**, 477 (1997).

[35] S. Goedecker, M. Teter, and J. Hutter, Phys. Rev. B **54**, 1703 (1996).

[36] G.J. Martyna and Mark E. Tuckerman, J. Chem. Phys. **110**, 2810 (1999).

[37] D.J. Tobias, G.L. Martyna, and M.L. Klein, J. Phys. Chem. **97**, 12959 (1993).